DNA Damage Enhancement from Gold Nanoparticles for Clinical MV Photon Beams

Ross I. Berbeco[a,1], **Houari Korideck**[a], **Wilfred Ngwa**[a], **Rajiv Kumar**[b], **Janki Patel**[b], **Srinivas Sridhar**[b], **Sarah Johnson**[c], **Brendan D. Price**[c], **Alec Kimmelman**[a], and **G. Mike Makrigiorgos**[a]

[a]Department of Radiation Oncology, Division of Medical Physics and Biophysics, Brigham and Women's Hospital, Dana-Farber Cancer Institute and Harvard Medical School, Boston, Massachusetts

[b]Department of Physics, Northeastern University, Boston, Massachusetts

[c]Department of Radiation Oncology, Division of Genomic Instability and DNA Repair, Dana-Farber Cancer Institute and Harvard Medical School, Boston, Massachusetts

Abstract

In this study, we quantify the relative damage enhancement due to the presence of gold nanoparticles (GNP) *in vitro* in a clinical 6 MV beam for various delivery parameters and depths. It is expected that depths and delivery modes that produce a larger proportions of low-energy photons will have a larger effect on the cell samples containing GNP. HeLa cells with and without 50 nm GNP were irradiated at depths of 1.5, 5, 10, 15 and 20 cm. Conventional beams with square aperture sizes 5, 10 and 15 cm at isocenter, and flattening filter free (FFF) beams were used. Relative DNA damage enhancement with GNP was evaluated by γ-H2AX staining. Statistically significant increases in DNA damage with GNP, compared to the absence of GNP, were observed for all depths and delivery modes. Relative to the shallowest depth, damage enhancement was observed to increase as a function of increasing depth for all deliveries. For the conventional (open field) delivery, DNA damage enhancement with GNP was seen to increase as a function of field size. For FFF delivery, a substantial increase in enhancement was found relative to the conventional field delivery. The measured relative DNA damage enhancement validates the theoretically predicted trends as a function of depth and delivery mode for clinical MV photon beams. The results of this study open new possibilities for the clinical development of gold nanoparticle-aided radiation therapy.

INTRODUCTION

Gold nanoparticles (GNP) are of interest for *in vivo* applications in radiotherapy due to their established biocompatibility (1, 2) and the high K-edge of gold (~81 keV) that can lead to the emission of short-range photoelectrons upon irradiation with low-energy photons. For example, Hainfeld *et al.* showed a remarkable improvement in local control in a mouse xenograft model with untargeted gold nanoparticles when combined with kilovolt (kV) photon irradiation (3).

Most of the previous theoretical studies have prematurely dismissed the potential of combining GNP with megavolt (MV) external beam irradiation by treating every part of the

[1]Address for correspondence: Department of Radiation Oncology, Brigham and Women's Hospital, 75 Francis St., ASBI-L2, Boston, MA 02115; rberbeco@lroc.harvard.edu.

tumor as an equally important target and by assuming a homogenous distribution of GNP throughout the tumor for modeling dose enhancement (4, 5). Accordingly, most previous reports rely solely on low-energy photon sources, a concept that is limited in a clinical setting due to either gross under-coverage of the tumor or very poor skin sparing in the patient. In contrast, we have shown that for gold nanoparticles in direct contact with endothelial cells, the expected local dose enhancement to those structures increases up to 100-fold over previous calculations (4–7). Focusing our attention on MV irradiation, the clinical standard, to specifically damage the tumor endothelial cells is a departure from the current trends in the field.

There are two previous studies that measured DNA damage enhancement at a single depth for a 6 MV beam (8, 9). Chithrani *et al.* found an enhancement of 1.17 for 50 nm GNP at 1.5 cm depth in tissue equivalent material. Jain *et al.* found an enhancement of 1.29 for 1.9 nm GNP at 5 cm depth (100 cm SSD) in tissue equivalent material. The same group was also able to develop a Monte Carlo method to reproduce this result (10). In the study presented here, the experimental work was extended to include several additional depths and beam aperture sizes, as well as a flattening filter free (FFF) delivery. The proportion of low-energy photons in a clinical MV photon beam depends on the depth in material. Beam "softening" will occur at deeper measurement points as the contribution of low-energy scattered photons becomes more significant relative to the attenuated primary beam. Therefore, we hypothesize that the damage enhancement will increase as a function of increasing depth. We also anticipate that the FFF beam delivery mode will further increase the fraction of these photons. Our previously published work was the first to recognize these as potential improvements to MV radiation therapy enhancement with gold nanoparticles (11), and this current work represents the first *in vitro* results confirming those hypotheses.

METHODS AND MATERIALS

Cell Culture

The human HeLa cell line was provided by the American Type Culture Collection (ATCC, Manassas, VA). Cells were routinely cultured in Dulbecco's modified eagle medium (DMEM) (Cellgro Laboratories, Manassas, VA) supplemented with 10% fetal bovine serum (Cellgro) and 100 Units/ml penicillin and streptomycin (Invitrogen, Carlsbad, CA). Cells were grown as monolayers at 37°C in a humidified atmosphere of 5% CO_2. Exponentially growing cells were seeded for overnight in an eight-well chamber slide (Nalge Nunc International, Rochester, NY) at a concentration of 4×10^4 cells/0.5 ml. Each chamber had a culture area of 0.7 cm^2.

Nanoparticle Formulation

The 50 nm spherical GNP, conjugated with methyl polymer, were purchased from Nanopartz, Inc. (Loveland, CO). Two different concentration of GNP (0 and 0.05 mg/ml) in complete DMEM were added to the HeLa cells and were incubated for 24 h. Well chambers with and without GNP were located side by side to enable simultaneous irradiation.

Irradiation

All irradiations were performed on a Varian 2100 EX clinical linear accelerator (LINAC) operating in the nominal 6 MV peak photon energy mode (Varian Medical Systems, Inc., Palo Alto, CA). The dosimetric output of the LINAC is calibrated monthly based on the procedure described in the AAPM TG-51 report using an ion chamber with direct traceability to an ADCL laboratory. A fixed source-to-axis distance (SAD) set-up was used for each treatment depth, so that the cells were always at the plane through the machine

isocenter and orthogonal to the central axis of the beam. The experimental setup is shown in Fig. 1.

The cell chamber plates were surrounded laterally by custom cut tissue-equivalent bolus material (Superflab) and with Plastic Water (CIRS, Inc., Norfolk, VA) above and beneath. At least 10 cm of material was placed beneath the cells to have sufficient material for backscatter. Irradiations were performed with the chambers centered on the central axis, in the same orientation at five different depths (1.5, 5, 10, 15 and 20 cm).

Conventional (open field) beams of symmetric jaw sizes 5, 10 and 15 cm were investigated, as well as FFF fields delivered with a 15 cm (square) jaw setting. The dose for every irradiation was matched to be 4 Gy at the measured depth. Dose rates were also matched to be 600 MU/min for all deliveries. The dose rate for the FFF delivery slightly exceeded this (12–25%), but not to a clinically significant extent (12). Sham (control) samples prepared at the same time were brought to the clinic, but were not irradiated. Measurements were repeated in duplicate.

Cell Fixation and Antibodies Staining

Four hours after irradiation, untreated control cells (nonirradiated) and irradiated cells were washed twice in phosphate buffer saline (PBS) before fixation in ice-cold methanol. Cells were stored in fixative for not more than 72 h before γ-H2AX antibody staining.

Fixed cells were rehydrated with three washes in PBS. Cells were blocked for 40 min at room temperature in a blocking buffer comprised of PBS containing 3% nonfat milk protein (Foodhold, Landover, MD) at 1:10.000 dilution. Cells were then incubated for 1 h at room temperature in anti-phospho-histone H2AX antibody mouse monoclonal (Millipore, Billerica, MA) diluted to 1:1000 in blocking buffer. Incubation with the second antibody, which was goat anti-mouse IgG-TR diluted to 1:1000 (Santa Cruz Biotechnology, Santa Cruz, CA), was performed for 40 min in the dark at room temperature. Cells were washed three times with PBS at the end of each step.

Fluorescent Microscopy

To stain the nuclei for imaging, 2 μg of DAPI (4,6-diamidino-2-phenylindole) (Carlsbad, CA) diluted in 200 μL of mounting media, Fluoromount G (Southern Biotech, Birmingham, AL) were added. Merged images of the nuclear staining (DAPI) and Texas Red signals for γ-H2AX foci were collected using fluorescence microscopy Axio imager-Z1 (Carl Zeiss MicroImaging, Inc., Thornwood, NY) with appropriate optical filters. Using 60-fold magnification objective, γ-H2AX foci were counted in the nuclei of at least 100 of the treated and untreated cells for each modality.

Each cell was scored as "positive" if more than five foci were visible, and "negative" if not (13, 14). The fraction R of "positive" cells was derived as follows:

$$R = \frac{\sum N_{>5\,foci}}{\sum N_{>5\,foci} + \sum N_{\leq 5\,foci}}. \quad (1)$$

This same calculation was carried out for the samples prepared with and without nanoparticles. The fraction of positive samples found in the sham samples were subtracted from the irradiated samples to find the damage enhancement factors:

$$DEF = \frac{R_{\text{GNP}} - R_{\text{sham w/GNP}}}{R_{\text{no GNP}} - R_{\text{sham w/o GNP}}}. \quad (2)$$

RESULTS

Using the student's *t* test, statistically significant ($P < 0.02$) damage enhancement was observed for all depths and delivery modes when GNP were included. The enhancement becomes more significant for larger depths for each of the delivery modes, indicating statistically significant depth dependence. However, the functional form of the increase in enhancement could not be determined from the experimental data, and therefore a linear representation is used in the figures. The results of the damage enhancement by modality are presented below.

Conventional Irradiation

Statistically significant ($P < 0.02$) damage enhancement was observed at each depth measured for all field sizes that were investigated. Relative to the shallowest depth, damage enhancement was observed to increase as a function of increasing depth for all field sizes (Fig. 2). The difference in field size was shown to produce a significant difference in the enhancement for all depths combined ($P < 0.01$). However, the separation between the 5×5 cm and 10×10 cm cases became insignificant at the deepest depths.

Flattening Filter Free Irradiation

For FFF delivery, a substantial increase in damage enhancement was observed as a function of depth (Fig. 3). This enhancement was significantly larger than the case of no GNP ($P < 0.001$) as well as in the case of conventional delivery ($P < 0.002$). The relative difference in enhancement between FFF and conventional delivery was found to be largest at the shallow depths and smallest at the greatest depths. This may be due to the competing effects of hardening of the inherently softer FFF beam and softening of the inherently harder conventional beam.

Control Groups

Analysis of the cell samples irradiated without GNP was conducted (Fig. 4), and it was observed that there is no systematic difference between each modality or as a function of depth.

Sham samples were used for each of the cases above to assess the damage enhancement due to the GNP without irradiation. The damage enhancement from the GNP, without irradiation, was 1.10 ($R_{\text{GNP}} = 0.21$, $R_{\text{no GNP}} = 0.19$). These results were taken into account as shown in Eq. (2)).

DISCUSSION

The hypothesis that GNP will increase DNA damage in an MV beam and that this enhancement is dependent on depth and delivery mode has been demonstrated. The results compare favorably with those of Chithrani *et al.* (8) and Jain *et al.* (9), who used similar conditions at single depths (1.5 and 5 cm, respectively). The additional depths and modalities studied here demonstrate that damage enhancement depends on treatment factors that affect the proportion of low-energy photons within the beam. The significant increase in damage with the flattening filter free delivery is particularly interesting, as this treatment modality is now commercially available and is currently becoming more clinically accepted.

Future studies will focus on the use of Monte Carlo methods to optimize the proportion of low-energy photons in the treatment beam while maintaining appropriate normal tissue sparing. Based on the trends found in this study, we anticipate that a rational approach for altering beam delivery parameters to maximize the therapeutic efficacy will further augment the potential for GNP-aided radiotherapy. This will be particularly powerful if appropriate radiosensitive or otherwise important substructures can be identified and targeted (e.g., tumor endothelial cells).

It is important to note that the damage enhancement found in this study may not necessarily translate directly to the clinical effect, which may be greater or less depending on *in vivo* biological and physiological cofactors. This *in vitro* study was only meant to show the relative change in damage enhancement for changing treatment parameters: depths, field sizes and with the flattening filter removed. The clinical advantage of GNP-aided radiotherapy will also depend on distribution and concentration of GNP, *in vivo* cellular uptake, biological target and subsequent physiological changes; e.g., vascular disruption (6, 15).

Collateral advantages of targeted gold nanoparticle-aided radiation therapy include the inherent image contrast enhancement associated with gold in X ray and CT imaging (3, 16–21), and the known suitability of GNP for attaching drugs and radiosensitizers (22–27). A targeted gold nanoparticle platform can be combined with precise imaging and synergistic compounds to further improve the safety and efficacy of radiation therapy. Therefore, the accumulated effects will amplify the clinical significance of this concept.

CONCLUSION

Relative increases of *in vitro* DNA damage enhancement have been shown for gold nanoparticle aided MV radiotherapy at increasing depths and by removing the flattening filter of the linear accelerator. Although the *in vitro* experimental setup is only an approximation of the proposed *in vivo* scenario of endothelial cell targeting, the measured relative damage enhancement validates the theoretically predicted dependence on the depth and delivery mode for a clinical MV beam. The results of this study open new possibilities for the clinical development of gold nanoparticle aided radiation therapy.

Acknowledgments

References

1. Lasagna-Reeves C, et al. Bioaccumulation and toxicity of gold nanoparticles after repeated administration in mice. Biochem Biophys Res Comm. 2010; 393(4):649–55. [PubMed: 20153731]

2. Khlebtsov N, Dykman L. Biodistribution and toxicity of engineered gold nanoparticles: a review of in vitro and in vivo studies. Chem Soc Rev. 2011; 40(3):1647–71. [PubMed: 21082078]

3. Hainfeld JF, Slatkin DN, Smilowitz HM. The use of gold nanoparticles to enhance radiotherapy in mice. Phys Med Bio. 2004; 49(18):N309–15. [PubMed: 15509078]

4. Cho SH. Estimation of tumour dose enhancement due to gold nanoparticles during typical radiation treatments: a preliminary Monte Carlo study. Phys Med Bio. 2005; 50(15):N163–73. [PubMed: 16030374]

5. Roeske JC, Nunez L, Hoggarth M, Labay E, Weichselbaum RR. Characterization of the theorectical radiation dose enhancement from nanoparticles. Tech Cancer Res Treat. 2007; 6(5):395–401.

6. Berbeco RI, Ngwa W, Makrigiorgos GM. Localized dose enhancement to tumor blood vessel endothelial cells via megavoltage x-rays and targeted gold nanoparticles: new potential for external beam radiotherapy. Int J Radiat Oncol Bio Phys. 2011; 81(1):270–6. [PubMed: 21163591]

7. Cho SH, Jones BL, Krishnan S. The dosimetric feasibility of gold nanoparticle-aided radiation therapy (GNRT) via brachytherapy using low-energy gamma-/x-ray sources. Phys Med Bio. 2009; 54(16):4889–905. [PubMed: 19636084]

8. Chithrani DB, et al. Gold nanoparticles as radiation sensitizers in cancer therapy. Radiat Res. 2010; 173(6):719–28. [PubMed: 20518651]

9. Jain S, et al. Cell-specific radiosensitization by gold nanoparticles at megavoltage radiation energies. Int J Radiat Oncol Bio Phys. 2011; 79(2):531–9. [PubMed: 21095075]

10. McMahon SJ, et al. Nanodosimetric effects of gold nanoparticles in megavoltage radiation therapy. Radiother Oncol. 2011; 100(3):412–6. [PubMed: 21924786]

11. Berbeco RI, Ngwa W, Makrigiorgos GM. Localized dose enhancement to tumor blood vessel endothelial cells via targeted gold nanoparticles: new potential for external beam radiotherapy. Int J Radiat Oncol Bio Phys. 2011; 81(1):270–6. [PubMed: 21163591]

12. Ling CC, Gerweck LE, Zaider M, Yorke E. Dose-rate effects in external beam radiotherapy redux. Radiother Oncol. 2010; 95(3):261–8. [PubMed: 20363041]

13. Xu Y, et al. The p400 ATPase regulates nucleosome stability and chromatin ubiquitination during DNA repair. J Cell Biol. 2010; 191(1):31–43. [PubMed: 20876283]

14. Camphausen K, et al. Enhanced radiation-induced cell killing and prolongation of gamma H2AX foci expression by the histone deacetylase inhibitor MS-275. Cancer Res. 2004; 64(1):316–21. [PubMed: 14729640]

15. Ngwa W, Makrigiorgos GM, Berbeco RI. Applying gold nanoparticles as tumor-vascular disrupting agents during brachytherapy: estimation of endothelial dose enhancement. Phys Med Bio. 2010; 55(21):6533–48. [PubMed: 20959684]

16. Hainfeld JF, Slatkin DN, Focella TM, Smilowitz HM. Gold nanoparticles: a new X-ray contrast agent. Br J Radiol. 2006; 79(939):248–53. [PubMed: 16498039]

17. Aydogan B, et al. AuNP-DG: Deoxyglucose-labeled gold nanoparticles as x-ray computed tomography contrast agents for cancer imaging. Molec Imag Bio. 12(5):463–7.

18. Kojima C, et al. X-ray computed tomography contrast agents prepared by seeded growth of gold nanoparticles in pegylated dendrimer. Nanotechnology. 21(24)

19. Boote E, et al. Gold nanoparticle contrast in a phantom and juvenile swine: models for molecular imaging of human organs using x-ray computed tomography. Academic Radiology. 17(4):410–7. [PubMed: 20207313]

20. Li J, et al. A novel functional CT contrast agent for molecular imaging of cancer. Phys Med Bio. 55(15):4389–97. [PubMed: 20647599]

21. Berbeco R, Korideck H, Yue Y, Makrigiorgos M. Gold nanoparticles as a contrast agent for in-treatment tumor tracking. Med Phys. 2011; 38(6):3476.

22. Shenoy D, et al. Surface functionalization of gold nanoparticles using hetero-bifunctional poly(ethylene glycol) spacer for intra-cellular tracking and delivery. Int J Nanomed. 2006; 1(1): 51–7.

23. Bergen JM, Von Recum HA, Goodman TT, Massey AP, Pun SH. Gold nanoparticles as a versatile platform for optimizing physicochemical parameters for targeted drug delivery. Macromolec Biosci. 2006; 6(7):506–16.

24. Paciotti GF, Kingston DGI, Tamarkin L. Colloidal gold nanoparticles: A novel nanoparticle platform for developing multifunctional tumor-targeted drug delivery vectors. Drug Devel Res. 2006; 67(1):47–54.

25. De M, Ghosh PS, Rotello VM. Applications of Nanoparticles in Biology. Adv Mater. 2008; 20(22):4225–41.

26. Duncan B, Kim C, Rotello VM. Gold nanoparticle platforms as drug and biomacromolecule delivery systems. J Contr Rel. 148(1):122–7.

27. Nagesha DK, et al. Radiosensitizer-eluting nanocoatings on gold fiducials for biological in-situ image-guided radiotherapy (BIS-IGRT). Phys Med Bio. 55(20):6039–52. [PubMed: 20858923]
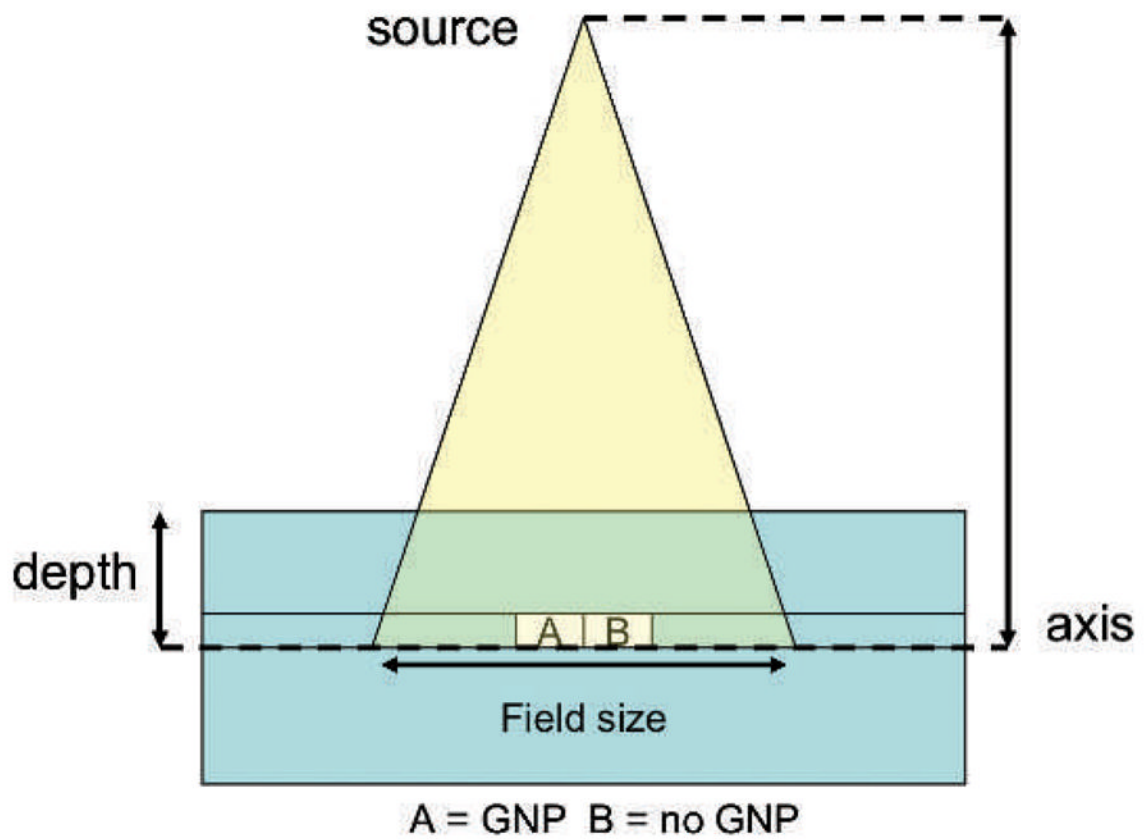
FIG. 1.
A side view of the experimental setup is shown. The source-to-axis distance (SAD) is kept at 100 cm. The chambers that contain cells are placed within a phantom (blue) consisting of tissue equivalent material. Chamber A has cells combined with GNP. Chamber B has no GNP.
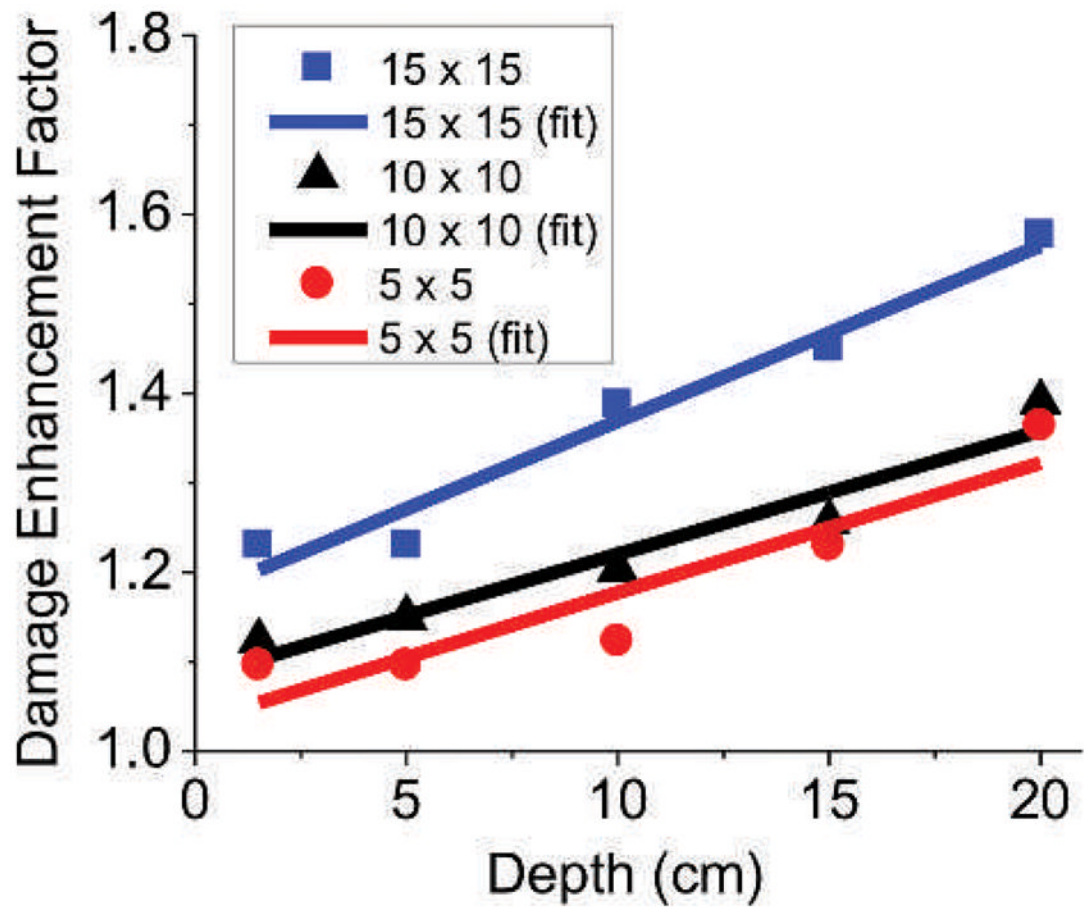
FIG. 2.
Damage enhancement as a function of depth in tissue-equivalent material for conventional (open field) photon field delivery with square apertures of size 5, 10 and 15 cm.
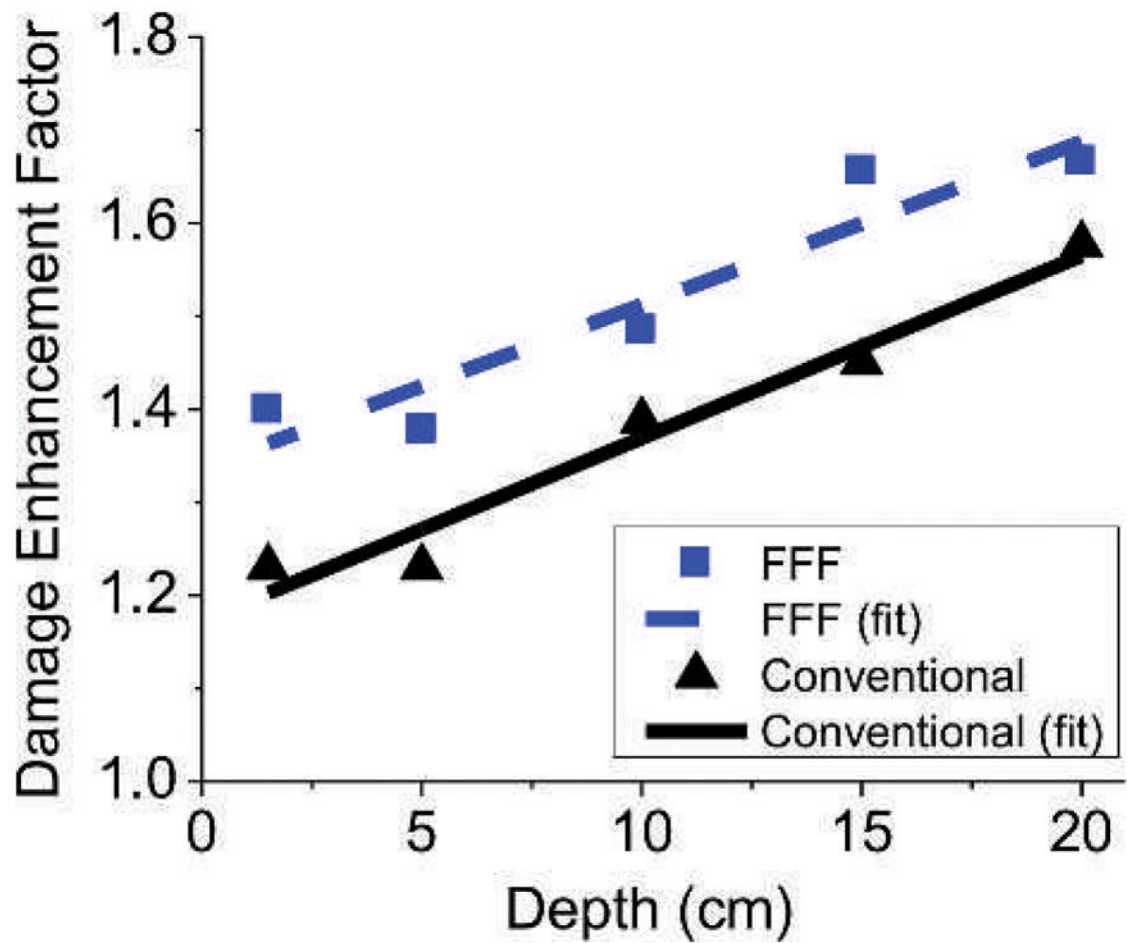
FIG. 3.
Damage enhancement as a function of depth in tissue equivalent material for conventional
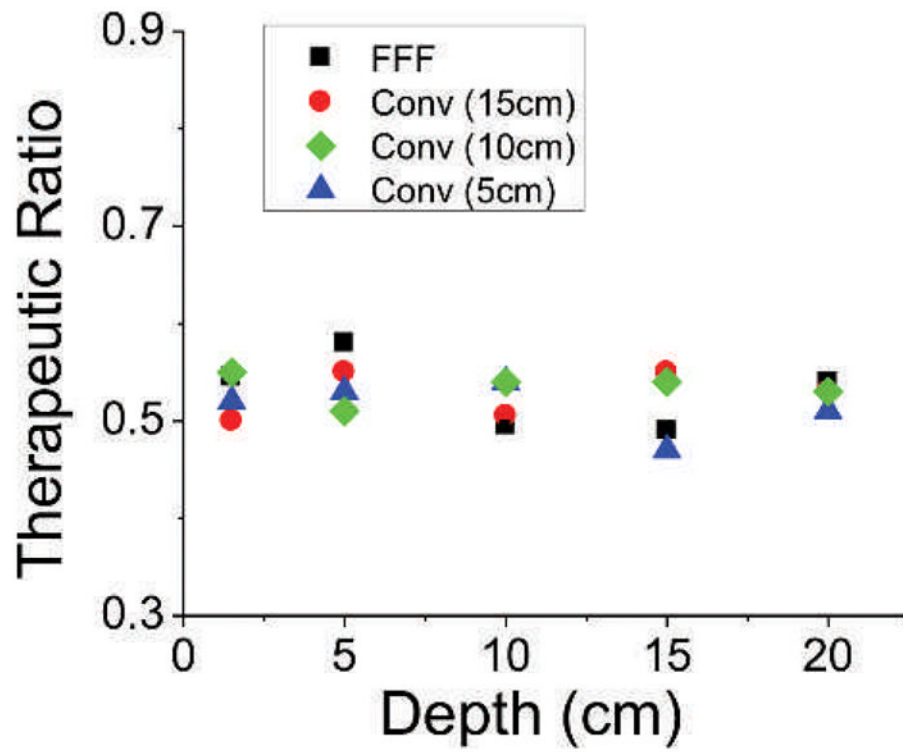(15 × 15 cm) and FFF (15 × 15 cm) photon field delivery.

FIG. 4.
The fraction of γ-H2AX positive cells without gold nanoparticles as a function of treatment depth. Results are shown for each of the irradiation conditions. No trend is observed.